RAA 2016 Vol. **16** No. **2**, 23 (8pp) doi: 10.1088/1674–4527/16/2/023
http://www.raa-journal.org *http://iopscience.iop.org/raa*

***R**esearch in*
***A**stronomy and*
***A**strophysics*

First generation solar adaptive optics system for 1-m New Vacuum Solar Telescope at Fuxian Solar Observatory

Chang-Hui Rao[1,2], Lei Zhu[1,2*], Xue-Jun Rao[1,2], Lan-Qiang Zhang[1,2], Hua Bao[1,2], Xue-An Ma[1,2], Nai-Ting Gu[1,2], Chun-Lin Guan[1,2], Dong-Hong Chen[1,2], Cheng Wang[1,2], Jun Lin[3], Zen-Yu Jin[3] and Zhong Liu[3]

[1] Key Laboratory on Adaptive Optics, Chinese Academy of Sciences, Shuangliu, Chengdu 610209, China; *zhulei_cas@aliyun.com*
[2] Laboratory on Adaptive Optics, Institute of Optics and Electronics, Chinese Academy of Sciences, Shuangliu, Chengdu 610209, China
[3] Yunnan Astronomical Observatories, Chinese Academy of Sciences, Kunming 650011, China

Received 2015 January 28; accepted 2015 August 17

Abstract The first generation solar adaptive optics (AO) system, which consists of a fine tracking loop with a tip-tilt mirror (TTM) and a correlation tracker, and a high-order correction loop with a 37-element deformable mirror (DM), a correlating Shack-Hartmann (SH) wavefront sensor (WFS) based on the absolute difference algorithm and a real time controller (RTC), has been developed and installed at the 1-m New Vacuum Solar Telescope (NVST) that is part of Fuxian Solar Observatory (FSO). Compared with the 37-element solar AO system developed for the 26-cm Solar Fine Structure Telescope, administered by Yunnan Astronomical Observatories, this AO system has two updates: one is the subaperture arrangement of the WFS changed from square to hexagon; the other is the high speed camera of the WFS and the corresponding real time controller. The WFS can be operated at a frame rate of 2100 Hz and the error correction bandwidth can exceed 100 Hz. After AO correction, the averaged residual image motion and the averaged RMS wavefront error are reduced to $0.06''$ and 45 nm, respectively. The results of on-sky testing observations demonstrate better contrast and finer structures of the images taken with AO than those without AO.

Key words: adaptive optics — high angular resolution — sunspots — granulation

1 INTRODUCTION

Adaptive optics (AO) systems, which provide correction to wavefront distortions introduced by the Earth's atmosphere, have become indispensable tools for ground-based solar telescopes when obtaining high-resolution solar images. The development of solar AO systems is more challenging than nighttime AO systems mainly due to worse daytime seeing and lower contrast in extended objects that must be used by the wavefront sensor (WFS) to detect wavefront aberrations (Rimmele et al. 2003).

The first AO experiments with the Sun were performed at the Dunn Solar Telescope (DST) by Hardy in 1979-1980 (Hardy 1980). The solar AO system developed by Lockheed (Acton & Smithson 1992) based on a Shack-Hartmann (SH) WFS was also tested at the DST. The development of a correlating SH WFS represented a breakthrough in solar AO, which enabled the tracking of granulation (Rimmele 2000). The first operational solar AO system was also based on a correlating SH WFS. Recently, both the 1.6-m NST and the 1.5-m GREGOR have developed their own low-order AO systems, and were subsequently followed by high-order ones (Berkefeld et al. 2010; Cao et al. 2010).

The development of a solar AO system in China can be traced back to the tip/tilt-correction system implemented in the 43-cm Solar Telescope of Nanjing University, which was successfully developed by the Institute of Optics and Electronics (IOE), Chinese Academy of Sciences in 2002 (Rao et al. 2003).

In 2008, a 37-element AO experimental system was successfully designed and built for the 26-cm solar fine structure telescope at Yunnan Astronomical Observatories, and saw its first light in September 2009 (Rao et al. 2010a,b). This system acted as a prototype for a meter-class solar AO system. This experimental prototype was modified and tested at the 1-m New Vacuum Solar Telescope (NVST) of Fuxian Solar Observatory (FSO) in 2011 (Rao et al. 2012). With support from the National Natural Science Foundation of China in 2012, the first generation solar AO system was developed. The configuration of the first generation solar AO system is almost the same as the aforementioned experimental prototype, other than

an update of the correlating SH WFS and the real time controller (RTC). Thanks to changes in the subaperture arrangement of the WFS, and increased speed of the WFS and the RTC, the spatial and temporal correction performances of the system are evidently improved. The configurations of the AO system are described in detail and the outcomes of the AO correction are shown in this paper. The contents of this paper are listed below. Section 2 gives an overview of the NVST. The AO system is introduced in Section 3. In Section 4, the performances of the AO system, including control characteristics, image motion error and wavefront error, are described. The observations of several active regions (ARs) are presented in Section 5. Section 6 provides a summary of current achievements and a discussion of the plan for future development.

2 OVERVIEW OF THE NVST

The 1-m NVST, located on the northeast shore of Fuxian Lake in Yunnan Province, China, was integrated and installed on-site in 2010 and its first light observation without AO was achieved on September 1 in the same year. The Fried parameter (r_0) of FSO obtained in the period from 1998 to 2000 was about 10 cm. At this observing site, the wind blows mostly from the lake with mean velocities of no more than 6 m s^{-1}. The sunshine duration of FSO is about 2200 hours per year (Liu et al. 2014; Liu & Xu 2011). The telescope is equipped with facility-class instruments including broad/narrowband filter imagers and a near-infrared spectrograph, to provide high-resolution imaging spectroscopy and polarimetry data in a spectral range from 0.3 μm to 2.5 μm.

Figure 1(a) shows a picture of the telescope and the optical configuration of NVST is presented in Figure 1(b). The optical design is an alt-azimuth mounted Gregory-Coudé type telescope: after the 1.2 meter diameter entrance window (W1), the primary mirror (M1) focuses light to F1; then the heat stop at F1 reflects most of the unused light out of the telescope and limits the field of view to 3 arcmin. The secondary mirror (M2) provides an effective focal ratio of F/9 and focus at F2, where a polarimeter can be inserted into the light path. The small flat mirror M4 is used to reflect light rays in the horizontal direction. M3 is a focusing mirror which converges light rays to the final focus at F3. The clear aperture of the telescope is 985 mm and the effective focal length before instruments are added is 45 meters (Liu et al. 2014).

3 FIRST GENERATION SOLAR AO SYSTEM

The AO system is composed of a fine tracking loop and a high-order correction loop. The optical layout and the design of these two loops are introduced as follows.

3.1 Optical Layout

Figure 2 illustrates the optical layout of the AO system, which is mounted after F3 in the telescope. Sunlight from the telescope is collimated into a beam with an aperture of 40 mm that is directed onto the tip-tilt mirror (TTM) and then the deformable mirror (DM) which is conjugated to the entrance pupil. The re-imaging optics system, which consists of two off-axis parabolic mirrors, collimates the beam into a 16 mm aperture and forms an image of the DM on the lanslet array of the SH WFS.

The first dichroic beam splitter transmits the beam at a wavelength of 500 nm to the correlation tracker camera as well as the correlating SH WFS. The imaging system mounted after the AO system permits simultaneous imaging in three channels: two channels are equipped with interference filters covering visible spectral regions at central wavelengths of 430.5 nm and 705.6 nm, respectively, and the third is equipped with an interference filter at a central wavelength of 1565.3 nm.

3.2 Fine Tracking Loop

The fine tracking loop is used to compensate image motion originating from mechanical vibrations and telescope guiding errors as well as random wavefront tilts averaged over the telescope entrance aperture which are caused by atmospheric turbulence. This loop is almost the same as that in the 37-element solar AO experimental prototype operated in conjunction with the 26-cm solar fine structure telescope of Yunnan Astronomical Observatories and described in the reference Rao et al. (2010b), except for the TTM which was newly manufactured by the IOE. The specifications of the TTM are listed as follows:

- Clear aperture: 58 mm;
- Tilt range: $\pm 4'$;
- Resonant frequency: about 1100 Hz;
- Original figure error: 0.0124λ PV and 0.020λ Root Mean Square (RMS) ($\lambda = 632.8$ nm).

3.3 High-order Correction Loop

The wavefront sensor of the high-order correction loop is a correlating SH WFS, which processes 30 subaperture images with dimensions 24 × 20 pixels. The 98 cm telescope aperture is sampled with seven subapertures across the pupil resulting in the subaperture size of 14 cm and the field of view of each subaperture is $12'' \times 10''$. The 37-actuator DM is also manufactured by IOE. The matching arrangement of the DM's actuators and the subapertures of the WFS is shown in Figure 3(b), in which the actuators and the subapertures are represented by circle symbols and the hexagon tessellation respectively. As a comparison, the arrangement of the WFS and the DM in the experimental prototype is also plotted in Figure 3(a). RMS errors of individual Zernike modes are used to qualify the correction ability of these two arrangements. The results shown in Figure 4 indicate that the AO system can efficiently compensate the first 20 Zernike modes. The AO system with the hexagon subapertures has a better correction capability than the system with the square subapertures.

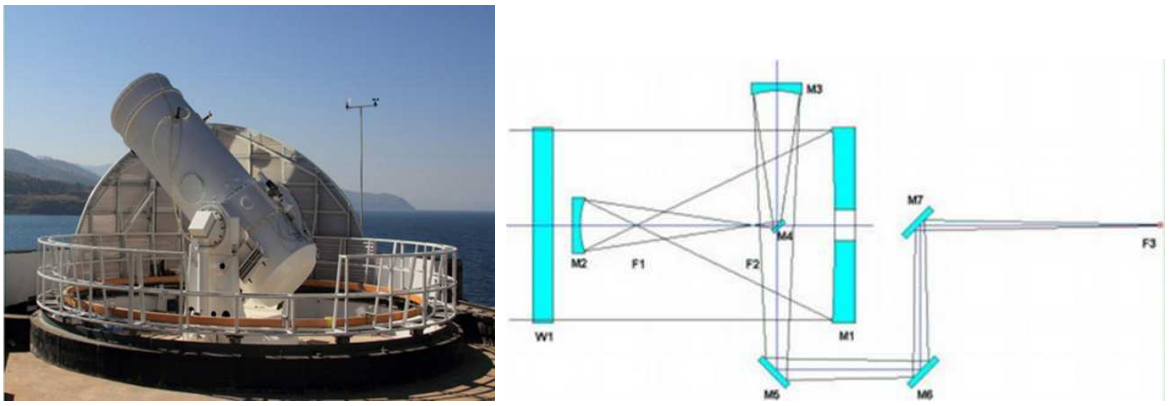

(a) (b)

Fig. 1 NVST and its wind screen (a) and the optical diagram of NVST (b).

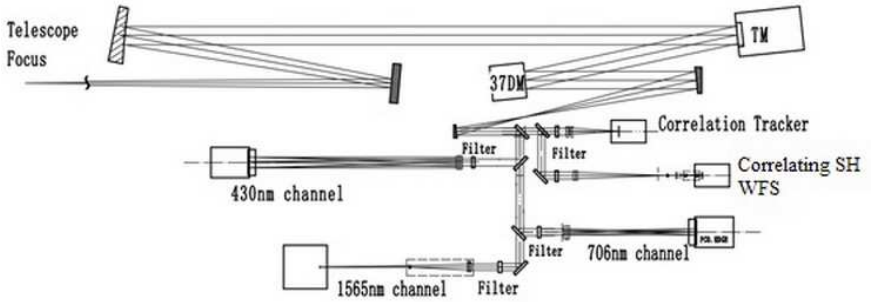

Fig. 2 Optical layout of the AO system.

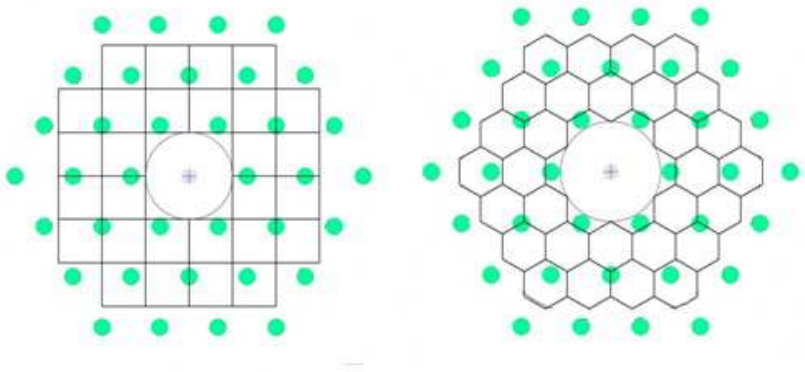

(a) (b)

Fig. 3 The matching arrangement of the actuators of DM and the subapertures of WFS. (a) The experimental prototype; (b) the updated AO system.

The optical layout of SH WFS is shown in Figure 5. It consists of a zoom lens, a field stop, a micro-lens array, relay optics, and a CMOS camera. The micro-lens array is conjugated with the DM. Before being mounted to the system, the SH WFS first needs to be integrated and calibrated using parallel light. The AO online diagnosis can be accomplished by replacing the field stop with a small pinhole at the prime focus of the telescope. If the common path optical aberrations of the AO system can be measured and corrected, the residual wavefront can be monitored. After AO correction, the far-field images can be focused precisely. Limited by the sampling frequency of WFS, the bandwidth of the experimental prototype system can only attain about 30 Hz, which cannot meet the requirement for temporal correction of the solar AO system. In the first generation solar AO system, the camera of the correlating SH WFS was updated to a high speed CMOS camera MC1362 manufactured by Mikrotron GmbH. The frame rate can be

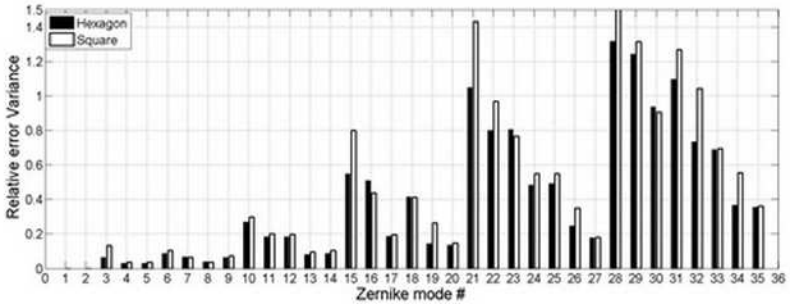

Fig. 4 The relative correction error (RMS) for the Zernike aberrations of the AO system.

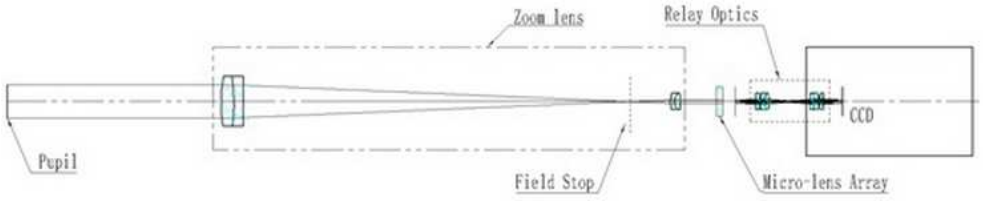

Fig. 5 The optical layout of SH WFS.

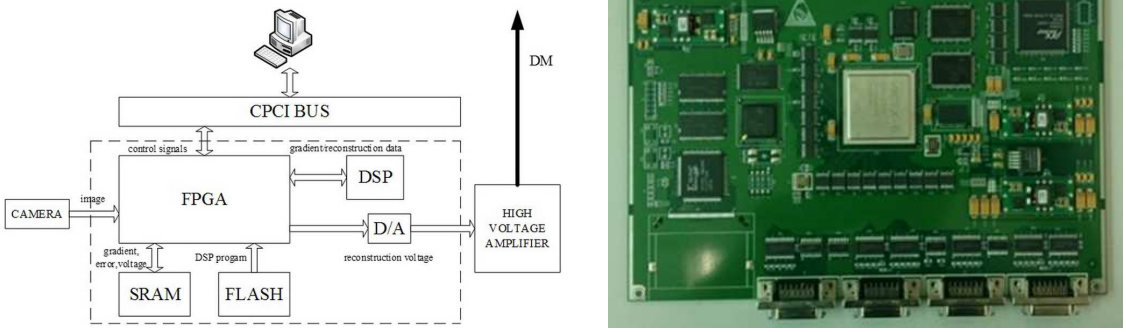

Fig. 6 Real time controller of the system. (a) Functional block diagram of RTC; (b) image of the circuit board.

operated at 2100 Hz for a readout of 180×160 pixels. The RTC was correspondingly updated to a new Xilinx FPGA and TI DSP (Zhu et al. 2012) to perform the following processing functions:

- Read subaperture images into the FPGA's processors;
- Apply flat and dark field corrections to the subaperture images;
- Calculate the x/y shifts of the subapertures based on the absolute difference algorithm;
- The minimum of each correlation is located to subpixel precision by fitting a parabola around the minimum pixel in DSP;
- Multiply the x/y shifts with the predetermined reconstruction matrix to compute actuator commands for the DM;
- Apply a PI servo algorithm to respond to actuator commands.

All of these functions are implemented in a single circuit board. Figure 6(a) shows the block diagram of the FGPA and DSP based RTC, and Figure 6(b) shows the image of the circuit board. Other main specifications of the high-order correction loop can be seen in Rao et al. (2012).

4 SYSTEM PERFORMANCE

Figure 7 shows the power spectrum (left panels) and its ratio (right panels) of closed-loop and open-loop data for selected Zernike modes corresponding to defocus (top) and astigmatism (bottom) of this AO system. The error rejection bandwidth of the AO system can exceed 100 Hz, which is much higher than that of the experimental prototype (30 Hz).

Figure 8 presents a time series of the measured open-loop and closed-loop image motion. The RMS value of the open-loop image motions are $0.68''$ and $0.47''$ in the X

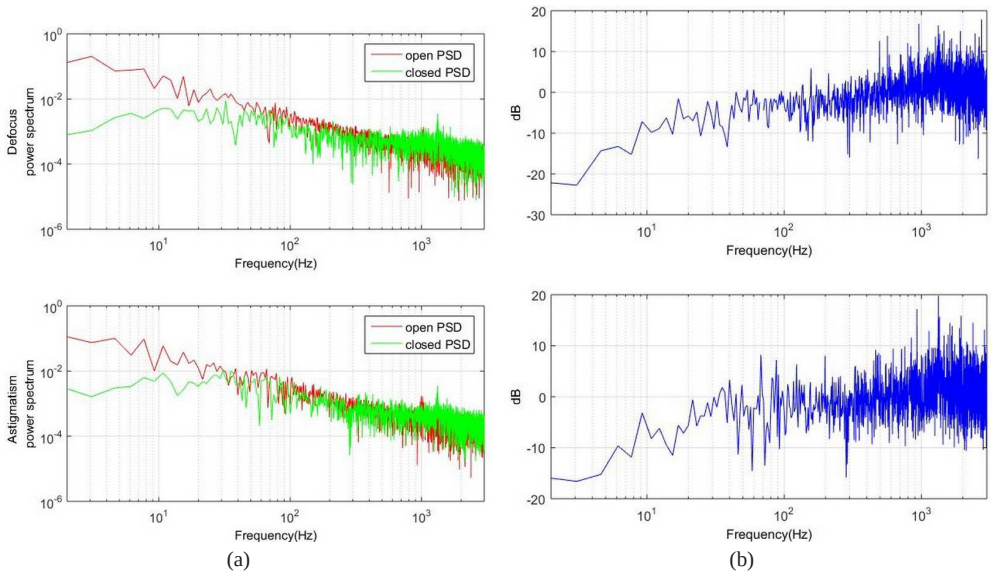

Fig. 7 Power spectra (a) and their ratio (b) of closed-loop and open-loop data for defocus and astigmatism modes of the AO system.

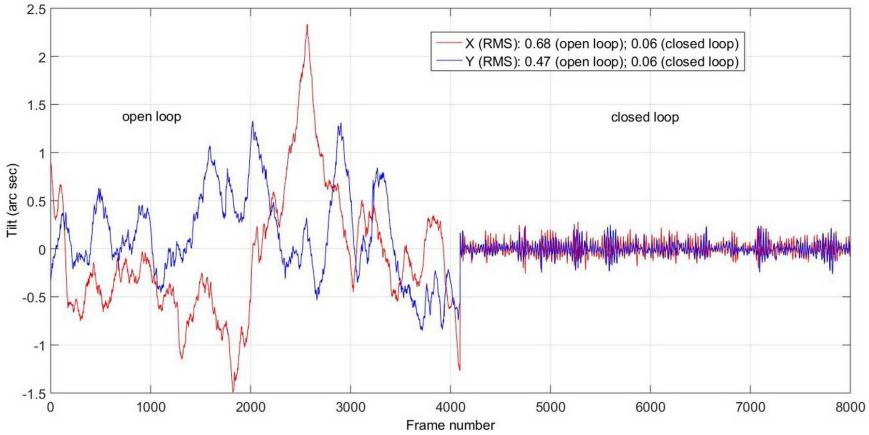

Fig. 8 The open-loop and closed-loop image motions of the AO system.

and Y directions respectively. As the fine tracking loop is closed-looped, the residual image motions are all reduced to $0.06''$ in both the X and Y directions. The results show the improvement of the correlation tracking is very evident and effective for image motion induced by atmospheric turbulence and mechanical vibrations from the telescope.

Figure 9 gives open/closed-loop wavefront error of the AO system. The results show that the wavefront error evidently decreased when the loop is closed. The open-loop averaged RMS wavefront error is about 236 nm without AO, but this value reduces to 45 nm after AO correction.

5 OBSERVATIONAL RESULTS

Solar observations using the new AO system were performed on 2013 June 16. Images of ARs NOAA 11768, NOAA 11769 and NOAA 11770 were simultaneously captured by two scientific CMOS cameras imaging at G-band 430.5 nm and TiO 705.7 nm, and an InGaAs camera at FeI 1565.7 nm. Images of the ARs NOAA 11769 and NOAA 11770 without AO and with AO are shown in the upper panels and lower panels of Figure 10 and Figure 11, respectively. It can be seen that the AO-corrected images have higher contrast and reveal finer structures, such as granules and penumbral filaments. Take the images of AR NOAA 11769 at TiO 705.7 nm as an example; the contrasts of Region A (sunspot) and Region B (granulation), as identified with boxes in Figure 12(a), in AO-off/on images were calculated. The contrasts of the sunspot and granulation are defined as

$$c_{\rm spot} = \frac{({\rm sub\_img})_{\rm max} - ({\rm sub\_img})_{\rm min}}{({\rm sub\_img})_{\rm max} + ({\rm sub\_img})_{\rm min}} \times 100\% \,, \quad (1)$$

$$c_{\rm granulation} = \frac{({\rm sub\_img})_{\rm std}}{({\rm sub\_img})_{\rm mean}} \times 100\% \,, \quad (2)$$

where the symbols $(...)_{\rm max}$, $(...)_{\rm min}$, $(...)_{\rm std}$ and $(...)_{\rm mean}$ signify the maximum value, minimum value, standard deviation and mean value of the matrix enclosed in parenthe-

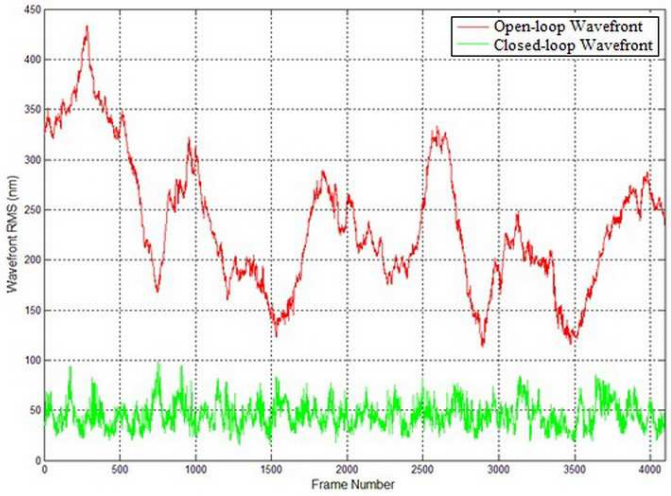

Fig. 9 Wavefront RMS error without AO (*in red*) and with AO (*in green*).

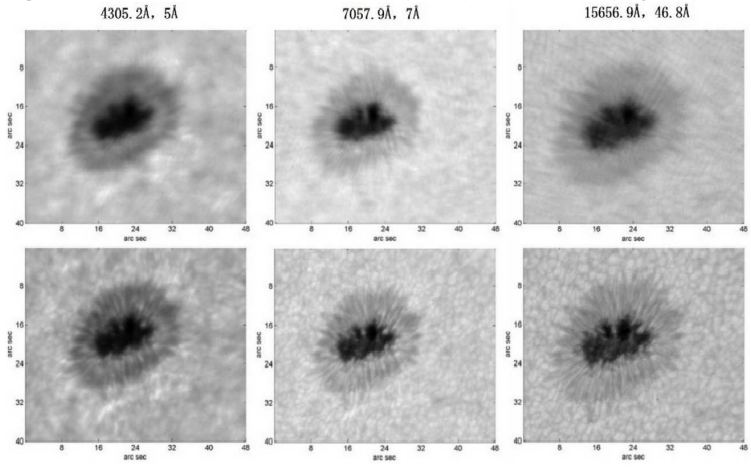

Fig. 10 Images of AR NOAA 11769 taken at G-band 430.5 nm, TiO 705.7 nm and FeI 1565.7 nm, from left to right respectively, without AO (*upper panels*) and with AO (*lower panels*).

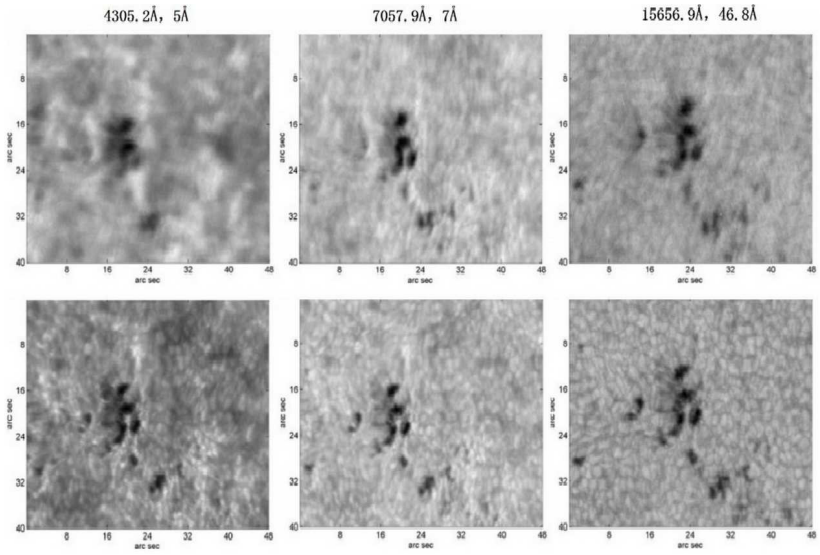

Fig. 11 Images of AR NOAA 11770 taken at G-band 430.5 nm, TiO 705.7 nm and FeI 1565.7 nm, from left to right respectively, without AO (*upper panels*) and with AO (*lower panels*).

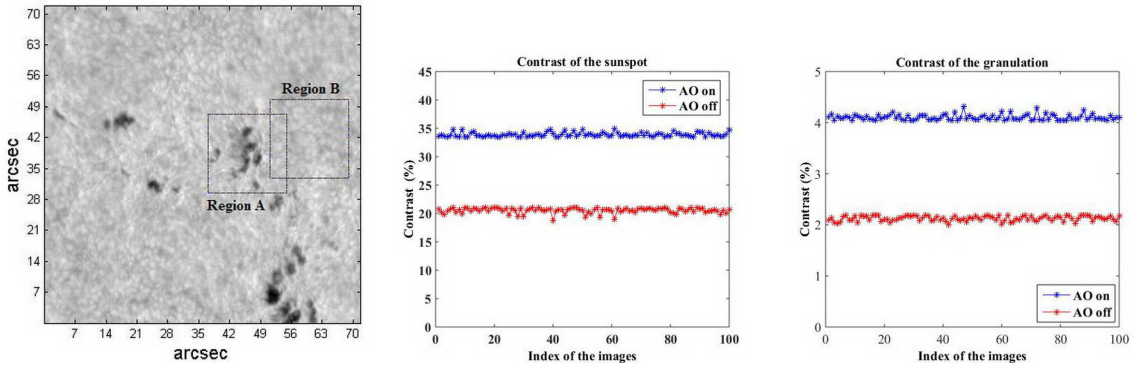

(a) (b) (c)

Fig. 12 An example AO-on image of the AR NOAA 11769 (a), the AO-off (*in blue*) /on (*in red*) contrast of the sunspot (b) and the AO-off/on contrast of the granulation (c).

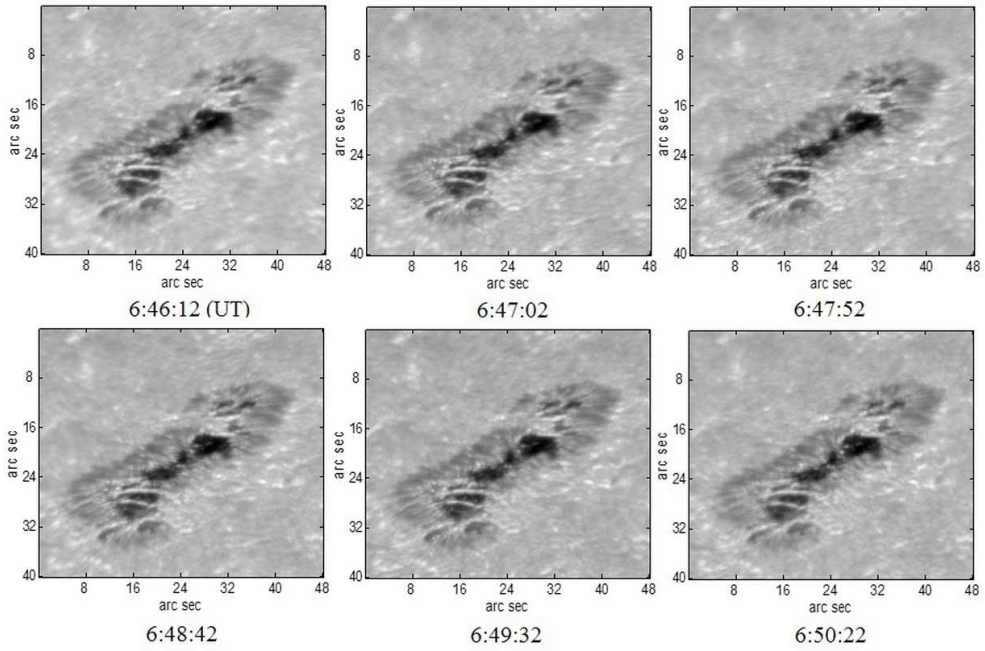

Fig. 13 Time sequence of TiO images of the AR NOAA 11768 with AO.

ses, respectively. A comparison of the AO-off and AO-on image contrast is shown in Figure 12(b) and 12(c).

With AO operating, a time sequence of images taken while observing the AR NOAA 11768 was acquired, as shown in Figure 13.

6 SUMMARY

The development of the NVST AO is divided into two steps. First, we successfully developed the low-order solar AO system (first generation) for NVST, which can compensate the low order Zernike modes and provides good results under excellent seeing conditions. The solar observational results have demonstrated that better contrast and finer structure can be obtained with the solar AO system than those without AO. Secondly, the next generation solar AO system, which is a 151-element high-order AO system, is already in progress and will enable diffraction limited observations in a wide range of seeing conditions. The NVST with our AO system is predicted to be scientifically productive when used with multi-wavelength high resolution imaging from visible to near infrared and the associated spectrometers.

Acknowledgements This work was funded by the National Natural Science Foundation of China (Grant No. 11178004). A special acknowledgement should be given to Prof. Wenhan Jiang from the Institute of Optics and Electronics, Chinese Academy of Sciences, for his revision from which we benefited greatly. In addition, we are also grateful to the reviewers for their valuable advice.

References

Acton, D. S., & Smithson, R. C. 1992, Appl. Opt., 31, 3161

Berkefeld, T., Soltau, D., Schmidt, D., & von der Lühe, O. 2010, Applied Optics, 49, G155

Cao, W., Gorceix, N., Coulter, R., et al. 2010, Astronomische Nachrichten, 331, 636

Hardy, J. W. 1980, Final Report, Feb. 1979-Jun. 1980 Itek Corp., Lexington, MA. Optical Systems Div., 1

Liu, Z., & Xu, J. 2011, in First Asia-Pacific Solar Physics Meeting ASI Conference Series, 2, 9

Liu, Z., Xu, J., Gu, B.-Z., et al. 2014, RAA (Research in Astronomy and Astrophysics), 14, 705

Rao, C.-H., Jiang, W.-H., Fang, C., et al. 2003, ChJAA (Chin. J. Astron. Astrophys.), 3, 576

Rao, C., Zhu, L., Rao, X., et al. 2010a, Applied Optics, 49, G129

Rao, C., Zhu, L., Rao, X., et al. 2010b, Chinese Optics Letters, 8, 966

Rao, C., Zhu, L., Gu, N., et al. 2012, in Society of Photo-Optical Instrumentation Engineers (SPIE) Conference Series, 8447, 46

Rimmele, T. R. 2000, in Society of Photo-Optical Instrumentation Engineers (SPIE) Conference Series, 4007, Adaptive Optical Systems Technology, ed. P. L. Wizinowich, 218

Rimmele, T. R., Richards, K., Hegwer, S. L., et al. 2003, in Society of Photo-Optical Instrumentation Engineers (SPIE) Conference Series, 4839, Adaptive Optical System Technologies II, eds. P. L. Wizinowich, & D. Bonaccini, 635

Zhu, L., Gu, N., Chen, S., et al. 2012, in 6th International Symposium on Advanced Optical Manufacturing and Testing Technologies (AOMATT 2012), International Society for Optics and Photonics, 84150V